Research Square

Preprints are preliminary reports that have not undergone peer review.
They should not be considered conclusive, used to inform clinical practice,
or referenced by the media as validated information.

# Buried Potential? Evaluating Long-Term Sequestration in a Restored Intertidal Habitat

**Eleanore Burrell**
*E.burrell-2020@hull.ac.uk*
University of Hull https://orcid.org/0009-0005-1543-376X

**Krysia Mazik**
*K.Mazik@hull.ac.uk*

**Hannah L. Mossman**
*h.mossman@mmu.ac.uk*
Manchester Metropolitan University

**Martin Taylor**
*Martin.Taylor@hull.ac.uk*

**Article**

**Keywords:**

**DOI:** https://doi.org/

**License:** This work is licensed under a Creative Commons Attribution 4.0 International License.
Read Full License

**Additional Declarations:** There is **NO** Competing Interest.

# Buried Potential? Evaluating Long-Term Sequestration in a Restored Intertidal Habitat

Burrell, E.J[1]., Mazik, K[1]., Mossman, H[2]., and Taylor, M[3]

[1]School of Environmental Science, University of Hull, Hull, United Kingdom. [2]Ecology and Environment Research Centre, Department of Natural Sciences, Manchester Metropolitan University, Manchester, United Kingdom. [3]School of Engineering, University of Hull, Hull, United Kingdom.

## Abstract

Restoration of intertidal habitats is increasingly promoted as a nature-based solution for climate mitigation, yet uncertainties remain around their carbon dynamics. This study provides the first full-depth, site-wide assessment of 20 years of sediment organic carbon (OC) accumulation in a UK restored intertidal habitat (Paull Holme Strays), based on 3,987 sediment samples across saltmarsh and mudflat. We integrate depth-resolved sampling, OC fractionation, and elevation-stratified modelling to quantify stocks and characterise variability. Since breaching in 2003, the site has accumulated ~125,000 $m^3$ of sediment, with 11–250 cm of elevation gain closely linked to initial elevation. OC declined non-linearly with depth (adj. $R^2 = 0.62$); labile OC was largely confined to an upper surface layers, while deeper layers were dominated by more persistent recalcitrant OC, consistent with breakpoint analysis. Elevation and depth were the primary correlates of OC variability, with bulk density and grain size acting as secondary influences. Annual OC accumulation averaged ~15 $t\,C\,ha^{-1}\,yr^{-1}$, with roughly one third labile and two thirds recalcitrant, reflecting the combined effects of sediment volume and carbon concentration. These analyses disentangled near-surface turnover from deeper, persistent storage and clarified why rapidly accreting, low-elevation areas with lower OC concentrations, and OC-dense high-elevation areas with limited accretion can yield comparable annual accumulation. An empirically defined surface horizon, paired with elevation-stratified, fraction-resolved profiles, provides a scalable basis for consistent comparison and strengthens transparent, standardised blue-carbon assessment.

## Introduction

Despite their relatively small spatial scale, saltmarsh and intertidal mudflats are globally significant carbon sinks, storing an estimated 0.4–6.5 Gt of organic carbon (OC) worldwide [1]. Alongside biodiversity support, flood protection and nutrient cycling [2], their capacity to

sequester atmospheric carbon dioxide makes them critical components of nature-based solutions in climate change mitigation [3, 4]. However, global saltmarsh and intertidal habitat extent continues to decline due to coastal development, sea-level rise, and increasing storm activity [5, 6]. Global net losses of ~76 $km^2$ $yr^{-1}$ between 2000-2019 reduced carbon burial capacity by an estimated 0.045 Tg $CO_2e$ $yr^{-1}$ [7].

In recognition of their functional and societal value, large-scale restoration and conservation efforts have been undertaken [8]. Over the past three decades, approximately 35 $km^2$ of intertidal habitat have been restored in the UK alone [9]. Across Europe, restoration is predominantly achieved through managed realignment (MR), which involves relocating flood defences landward and reinstating tidal flooding to previously reclaimed land [10]. MR sites are often low lying within the tidal frame due to land compaction and relative sea level rises following reclamation, meaning they often have substantial accommodation space for sediment accretion [11]. Following tidal reinstatement, rapid deposition of allochthonous carbon-rich sediment facilitates development [12], with OC sequestration shifting over time from burial of external inputs to plant-driven autochthonous accumulation as elevation increases [13]. Realigned intertidal habitats often differ from existing/natural systems in both biotic and abiotic characteristics due to historic land uses, including reduced porosity, altered drainage, and more anoxic subsurface conditions, shaping long-term sediment dynamics, redox potential and vegetation development [14, 15].

The largest carbon deposits in intertidal habitats are in the sediment [16], and its long-term persistence depends not only on rates of accumulation but also on the extent to which deposited carbon is protected from remineralisation [17]. Waterlogged, anoxic conditions in sediments slow down organic matter decomposition, enhancing long-term OC preservation [18]. The effectiveness of these preservation processes varies greatly among sites and is influenced by regional environmental controls such as sediment supply, tidal regime [19], vegetation composition [20], hydro-geomorphic setting [21], and marsh age [22].

While previous research has demonstrated the potential for restored coastal and estuarine systems to sequester OC [3, 4, 23], reported values vary widely between sites on a global scale (1.8–19.4 t C $ha^{-1}$ $yr^{-1}$) [1], reflecting both genuine spatial heterogeneity and methodological inconsistencies. Estimates at both local and national scales often rely on global averages of OC accumulation rates [24], commonly based on total organic carbon (TOC) measurements [25], or from limited datasets with surface extrapolations [26, 27]. Such approaches provide little insight into how carbon readily degraded by microbes, known as labile carbon, declines with depth, or how recalcitrant carbon that resists decomposition persists over decadal timescales [28]. This uncertainty in persistence and

long-term sequestration potential of OC in restored intertidal habitats limits the robustness and reliability of current estimates for inclusion in carbon markets and climate policy frameworks.

Here, we present the first high-resolution assessment of OC accumulation across a restored intertidal habitat in the UK, Paull Holme Strays. Drawing on 3987 sediment samples, collected across both vegetated saltmarsh and intertidal mudflat, we aim to (1) quantify site-level OC stocks and habitat-specific accumulation rates since creation in 2003; (2) characterise vertical OC profiles, partitioning labile and recalcitrant fractions, to quantify the extent and rate of labile organic carbon loss with depth; (3) identify an empirically defined surface layer to enable consistent spatial comparisons across heterogeneous elevations; and (4) test how environmental characteristics such as elevation, which influence sediment and allochthonous carbon supply [11], and sedimentary characteristics such as grain size, that affect the preservation of OC stock [20], correlate with OC variability. By explicitly distinguishing saltmarsh and mudflat contributions, we aim to reduce methodological bias from prescribed depths or full-core averaging and provide a reproducible framework for restored intertidal systems. While site-specific, our findings have broad relevance across NE Atlantic saltmarsh systems and provide a robust empirical foundation for developing accurate, standardised protocols for OC stock assessments.

# Methods

*Study site*

Sediment samples were collected from the MR site (Figure 1; 53°44′N, 0°16′W), located on the north bank of the Humber Estuary, UK. Breached in September 2003, it was the first MR site on the Humber and was designed to serve a dual role of coastal flood protection and habitat restoration due to coastal defence works and sea level rise [29]. The site was created by breaching the existing sea wall in two locations (Figure 1 a and b) restoring ~80 ha of intertidal habitat, part of which compensates for habitat loss elsewhere in the estuary. The site lies adjacent to Paull Holme Sands mudflat and forms part of a landscape covered by several national and international conservation designations [30].

*Quantifying sediment deposition and erosion*

Multiple Digital Terrain Models (DTMs) derived from airborne LiDAR data at 50 cm horizontal resolution [31] were obtained for the MR site at Paull Holme Strays. DTMs were available for the years 2003 (immediately post-breach) and for; 2004, 2005, 2007, 2010, 2012, 2013, 2014, 2016, 2017, 2019, and 2022. Where multiple flights existed, data was selected from similar seasons to minimise seasonal variations, such as dewatering or sediment reflocculation. The raster geoprocessing tool in ArcGIS Pro 3.3 was used to merge downloaded DTM tiles before being clipped by the MR site area (defined manually with a polygon around the crest of the flood

embankment). The first DTM available after the breach (26/09/2003) was clipped by the site boundary, and the resulting polygon (with an area of 79.8 ha) used to clip the remaining DTMs. Elevation change (in metres relative to Ordnance Datum Newlyn, m ODN) between DTMs was calculated to estimate net sediment accretion or erosion over time. Mean elevation change across raster pixels was calculated and then converted to total change in sediment volume by multiplying by the area covered by the raster DTM. Naturally accreted marsh areas that have risen above the highest astronomical tide were retained in the analysis, as these areas are part of the system's development and reflect long-term sediment and carbon accumulation processes. Any artificially elevated features such as the flood embankment were excluded from analysis of marsh sediment dynamics.

*Field sampling design*

Elevation varied considerably across the site as a function of initial elevation pre restoration elevation, combined with flooding, drainage and sedimentation dynamics over the past two decades. To capture this variation, we selected three sampling elevation bands, stratified by elevation from the 2022 lidar-derived DTM and in-situ vegetation composition (Figure 1a). High elevation bands comprised current elevations > 3m ODN, with dense vegetation including *Juncus maritimus, Phragmites australis*. Mid elevation bands comprised current elevations 2.5-3m ODN, with vegetation including *Cochlearia officinalis, Puccinellia maritima*, and Low elevation bands comprised current elevations <2.5m ODN, consisting of mainly bare mud with sporadic *Salicornia spp and Spartina anglica*. An area of approximately 3.4 ha near the eastern breach was modified in 2021/22 by the Yorkshire Wildlife Trust, involving excavation and adjacent piling of soil to create nesting habitat for Marsh Harriers and Redshank (pers. comm.). This activity altered the sediment surface through both removal and addition of material, but resulted in no net loss overall, so LiDAR-derived elevation calculations were unaffected. However, no sediment cores were collected from this area

Twenty-four sampling locations were randomly selected at each elevation band. In addition, a further six sampling locations were selected in the pre-existing saltmarsh seaward of the MR, with plant communities similar to those within the MR, to act as a natural reference (Figure 1a). At each sampling location, three replicate sediment cores (internal diameter 10cm) were taken to the depth of the pre-restoration agricultural surface, i.e. the full depth of the sediment accreting since restoration. This core length was calculated based on elevation change at each sampling stations from the differences in the 2003 and 2022 DTMs (Figure 1b). Sediment cores were sampled at each location between April and September 2023.

*Sediment collection*

Cores up to 1.2m depth were collected by hand, with a PVC core, 10cm internal diameter, a wall thickness of 0.5cm, and length of 1.5m, with

sharpened edges to cut through root material. Cores over 1.2m were collected with a vibrocore, using aluminium cores (7.6cm in diameter, 3m in length). The height of the corer above the sediment was measured on the outside, for calculating core penetration, and on the inside for estimating core compaction. In cases of minimal compression (<2cm), cores were retained, and compaction correction factor applied [32]. If compression was >2cm, the corer could not be inserted to the required depth, or there was significant sample loss another core was taken in close proximity.

*Sediment preparation*

All cores were processed the day of collection and sub sectioned into 5 cm lengths, to quantify variation in sediment carbon. In total 234 cores were collected, ranging in length from 40 to 250cm, resulting in 3987 samples. Each subsample was analysed in triplicate for physical and chemical properties; replicate measurements were averaged to minimise instrument-level variability before statistical analysis

Dry bulk density (sediment density) was determined by drying 30$cm^3$ of each of the 3987 sediment subsamples to a constant weight at 60˚C for 72 hours [33]. At temperatures exceeding 60˚C, fractions of sediment organic matter may oxidise and cause an under-estimation of OC [34]. Dry bulk density (DBD), the relationship between the mass of the dry solids (*M*) and the volume (*V*), was calculated from the equation DBD(g/l)=*M(g)/V(l)* [35].

*Sediment particle size analysis*

Dried sediment samples were treated with 10% hydrogen peroxide to remove organics, and further treated with 3% sodium hexametaphosphate (Calgon) as a dispersant [36]. After treatment, samples were stirred and sonicated for 15 minutes to aid disaggregation. A subsample was analysed for grain size using laser diffraction with a Malvern Mastersizer Hydro 2000 MU (Malvern, Worcestershire, UK), with three replicate measurements per sample. The instrument measured particle sizes across a 0.017–2000 µm range, reporting full particle size distributions and volumetric sand, silt, and clay fractions (sediment classes). Grain size statistics were calculated using the graphical method of Folk and Ward [37] graphical method on the logarithmic phi scale in GRADISTAT [38]. For analysis, we used: 1) mean grain size as the geometric mean (µm), obtained by back-transforming the phi-scale mean, and 2) sand, silt and clay fractions following the Wentworth scale as implemented in GRADISTAT. Because sand, silt, and clay percentages are compositional data (summing to 100%), fractions were transformed using the centred log-ratio (CLR) transformation prior to analysis.

*Quantifying organic carbon content of the sediment*

Total organic carbon content (TOC) analysis was performed using Elemental Analysis LECO CHN628 (LECO Corporation, USA), calibrated using EDTA as a standard. Dried, ground and sieved sediment samples (63 μm) [39] were weighed into tin foil cups, sealed and combusted in the presence of oxygen (Air Liquide, 99.999%) to generate $CO_x$, $NO_x$ and $H_2O$ at 950 °C. Total carbon was reported as wt.% mass of initial sample [40, 41]. Aliquots of the same samples analysed for TC were weighed and heated to 550˚C for 4 hours, at this temperature, carbon is removed leaving the inorganic carbon in the ash [42]. The ash was weighed to the nearest milligram and analysed on the Elemental Analyser (as outlined above) to determine the inorganic carbon content of the ash. The inorganic carbon content of the original sample was calculated by scaling the elemental analyser result by the ratio of ash weight to original dry weight. Organic carbon content (%) was then derived by subtracting the inorganic carbon from the total carbon content of each sample.

*Calculation of organic carbon stock*

Sediment organic carbon stocks were calculated from full-depth cores sampled at 5 cm intervals using 5 cm depth intervals, dry bulk density (DBD), and total organic carbon (TOC). For each subsample, SOC density ($g\,C\,cm^{-3}$) was calculated as:

$$\text{SOC density (g OC cm}^3\text{)} = \text{DBD (g cm}^{-3}\text{)} \times \frac{\%OC}{100}$$

The organic carbon content of each subsample was multiplied by its thickness and summed across the core to obtain per-core stocks, which were then converted to $t\,OC\,ha^{-1}$. Site-level mean stocks and standard deviations were calculated across cores, and average annual SOC accumulation ($t\,C\,ha^{-1}\,yr^{-1}$) was estimated by dividing core stocks by site age (19 yr). Site-wide accumulation was calculated using mean per-core values multiplied by total site area (78.9ha).

*Thermogravimetric analysis*

Dried and milled sediment samples were analysed using thermogravimetric analysis (TGA) to partition OC into labile and recalcitrant fractions. Analyses were conducted using a Thermogravimetric Analyzer LECO TGA701 (LECO Corporation, USA) under a constant flow of $N_2$, with samples heated from ambient temperature to 950 °C ([*Moisture Phase* - ambient to 107 °C at 3 °C/min, holding for 15 min], [*Volatile Phase* - 107-950 °C at 5 °C/min, holding for 7 min] and [*Ashing Phase* - 950-600 °C in nitrogen, followed by 600-750 °C in air at 3 °C/min before cooling to room temperature]). Labile OC was quantified as the mass loss between 200–400 °C, representing thermally unstable compounds, while recalcitrant OC was quantified as the mass loss between 400–650 °C, representing more stable organic matter. The proportion of each fraction was expressed relative to the total OC detected by TGA. Labile and recalcitrant OM densities were calculated in the same way as SOC density, detailed above.

# Data analysis

All statistical analyses were conducted using R software version 4.3.2 [43]. Data exhibited a moderate positive skew (SK = 0.617), and slight platykurtosis (K = 0.5), and remained non-normal despite transformation. Figures were produced using “ggplot2*”* [44]. Full code and model outputs are provided in the Supplementary Information.

*Site sediment deposition and erosion*

Spatial variation in accretion was modelled using Generalised Additive Models ( “mgcv” package, Wood [45]), based on the initial post-restoration elevation surface (2003), which was classified into three zones: Low (<2.5 m ODN), Mid (2.5–3.0 m ODN), and High (>3.0 m ODN). Thin plate regression splines were used to capture non-linear accretion trajectories across zones.

*Sediment Properties and Organic Carbon Profiles*

Sediments properties were modelled as a function of elevation zone, and depth within the core. Organic carbon (total, labile and recalcitrant (%)), bulk density (g $cm^{-3}$), sediment composition (sand/silt/clay%), and median grain size (µm) were modelled using GAMs fitted with the bam() function in the mgcv package [45]. Each model included elevation band as a fixed factor, smooth terms for non-linear depth profiles within elevations, and random intercepts for cores. To account for autocorrelation among successive depth increments, an AR(1) correlation structure was applied to model residuals. Smoothing parameters were estimated via fREML, and model adequacy was confirmed using residual diagnostics (gam.check). Model selection was based on Akaike Information Criterion (AIC), likelihood ratio tests, and cross-validation, with residual diagnostics assessing fit.

*Organic Carbon Stock and Accumulation Rates*

Uncertainty in site-scale OC accumulation was estimated using non-parametric bootstrapping (100,000 resamples) using the *boot* package [46]. Mean accumulation rates were calculated per unit area and scaled to the total site (78.9 ha) to estimate annual carbon sequestration (t C $yr^{-1}$) with associated 95 % confidence intervals.

*Evidence Based Surface Depth for OC Analysis*

Prescribed-depths or full-core averages, used in many studies can obscure or bias spatial comparisons because vertical accretion varies within and between intertidal habitats. We therefore defined a representative surface layer using a data-driven procedure informed by 3,987 samples to enable robust spatial comparisons across the site. Specifically, we combined four approaches: (1) the depth range exhibiting the greatest heterogeneity in sediment properties, bulk density (g $cm^{-3}$), grain size (µm), and sediment composition (sand/silt/clay%); (2) the inflection point marking stabilisation of labile OC with depth; and (3) the core depth encompassing ≥90% of cumulative OC. The median of these three estimates was taken to reduce bias from any single method; and (4) finally, segmented regression was applied to the site-aggregated profile of labile OC (median values per 5 cm interval) to identify a statistically significant breakpoint where the rate of labile OC decline changes, representing the transition from dynamic surface sediments to more stable subsurface layers.

# Results

*Sediment deposition and erosion*

Since its creation, the MR site has undergone substantial elevation gain, with approximately 125,111 $m^3$ of sediment accumulated (Figure 1b). Accretion varied considerably across the site (11-250 cm) and was strongly associated with initial pre-restoration elevation (GAM: adjusted $R^2$ = 0.78, deviance explained = 81.3%; edf = 7.16, F = 8.71, $p < 0.001$). Areas with low initial elevations exhibited both higher rates and greater spatial variability in sediment deposition, where elevation gains ranged from 40 to 250 cm. The largest gains occurred near the western breach (Figure 1b), where adjacent low-lying areas accumulated sediment rapidly, consistent with site morphology and tidal exposure. In contrast, areas with higher initial elevations, such as near the new sea wall at the back of the marsh, showed the lowest elevation gains, ranging from 11 to 79 cm.

*Sediment Properties*

Bulk density, grain size, and sand–silt–clay composition, exhibited significant spatial variation across elevation bands and with depth across the site (see Supplementary Table 1 for full GAM outputs; Figure 2).

Bulk density was significantly lower in Low ($\beta = -0.130 \pm 0.016$, $p < 0.001$) and Mid elevations ($\beta = -0.030 \pm 0.015$, $p < 0.05$) compared to High elevations (median ± SE = 1.01 g $cm^{-3}$± 0.07 g $cm^{-3}$); there was no

significant difference between High and reference sampling stations (Figure 2a). Depth-related variation was also significant, with non-linear declines detected in all bands (edf = 5–7, $p < 0.001$). The highest densities occurred in the upper 15 cm of High-elevation cores (0.8–1.5 g $cm^{-3}$), while deeper layers were consistently less dense.

Grain size and textural composition showed contrasting spatial patterns. Low-elevation sediments were coarser (median = 9.36 µm) than High elevations (7.43 µm), consistent with GAM estimates ($\beta = +1.60 \pm 0.17$, $p < 0.001$). Grain size generally decreased with depth across all elevations ($p < 0.001$), with the most pronounced changes in Mid elevations (range: 5.1–11.3 µm). The coarsest layers were concentrated in the upper 10 cm of Low-elevation cores, while High-elevation cores were more homogeneous throughout the profile. Textural fractions reflected these trends: Low elevations had higher silt (86%) and lower clay (9%) compared to High elevations (14% clay) and Mid elevations (~10%). GAM outputs indicated significant differences between elevations for sand, silt, and clay (all $p < 0.001$), with non-linear depth trends most pronounced for silt in Mid elevations (edf = 10.65, $F = 6.82$, $p < 0.001$) and clay in High elevations (edf = 8.95, $F = 3.72$, $p < 0.001$). Non-linear patterns with depth indicate rapid changes in the upper layers and more stable conditions below ~30–40 cm, with Mid elevations increasingly resembling those of lower lying areas, particularly in grain size, whereas High-elevation cores remained more distinct, retaining higher bulk density and finer grain size (Figure 2c and d). This pattern suggests that deeper Mid-elevation sediments may represent older deposits laid down under hydrological conditions similar to those currently observed in Lower elevations.

*Organic Carbon Content and drivers of variation*

OC content declined significantly with depth across the site (adj. $R^2$ = 0.631; deviance explained = 65%). High (edf = 5.43, $F = 45.12$, $p < 0.001$) and Mid elevations (edf = 5.91, $F = 24.81$, $p < 0.001$) exhibited pronounced curvature, consistent with complex OC accumulation and decomposition through the sediment profile (Figure 3). Low elevations showed weaker, more gradual changes (edf = 2.55, $F = 12.06$, $p < 0.001$), while the Reference marsh displayed moderate non-linearity (edf = 2.95, $F = 14.14$, $p < 0.001$).

Models confirmed elevation (as of 2022) and depth (change in elevation since restoration) were the primary controls on OC content (%) (adj. $R^2$ = 0.62; deviance explained = 64%, see table S4 and S5). Consistent with site-wide depth declines (Figure 3), the significant elevation–depth interaction (edf = 11.8, $p < 0.001$) indicates that OC losses with burial were steepest in High elevations, where rapid accretion and vegetation inputs created carbon-rich surface layers, while Low elevations showed more gradual declines. Bulk density and grain size had weak or non-significant effects when elevation and depth were included, suggesting

their influence is largely mediated by these primary drivers. When elevation and depth were removed, both properties became significant predictors (bulk density: edf = 2.04, F = 10.1, $p < 0.001$; grain size: edf = 1.21, F = 18.4, $p < 0.001$), but explanatory power dropped (adj. $R^2$ = 0.50), confirming they act as secondary, correlated controls rather than independent drivers of OC.

Substantial heterogeneity among cores within elevation bands was captured (edf = 71.46, F = 13.20, $p < 0.001$), indicating fine-scale variability beyond elevation-level trends. Parametric contrasts confirmed significantly lower median OC in Low ($\beta = -0.680 \pm 0.083$, $p < 0.001$) and Mid ($\beta = -0.576 \pm 0.083$, $p < 0.001$) elevations relative to High, whereas differences for the Reference marsh were smaller and not statistically significant ($\beta = -0.273 \pm 0.153$, $p = 0.075$). Despite these trends, some low-lying areas retained substantial carbon stocks, particularly adjacent to the western breach (Figure 4), where stronger tidal currents during early post-breach stages promoted rapid and substantial deposition of organic-rich sediment in areas excavated during construction, leading to the greatest elevation gains across the site (Figure 1b). Total OC (integrated over depth) from cores in this area ranged from 1.8 to 4.1 g OC $cm^{-2}$, among the highest concentrations recorded across the site (0.8 – 6.56 1 g OC $cm^{-2}$). Conversely, much lower OC stocks were recorded at the eastern end of the site, where the breach is smaller and initial elevations were higher, limiting tidal exchange and sediment deposition. As a result, elevation gains were minimal (Figure 1b), and total OC typically remained below 3 g $cm^{-2}$. The highest total OC stocks were observed in the higher-elevated, densely vegetated areas at the western end of the site (Figure 4). Cores from these elevations frequently exceeded 3.8% OC in the top 30cm of sediment, with total OC stocks site-wide ranging between 3.0 and 6.6 g $cm^{-2}$. These high stocks occurred in areas that experienced substantial elevation gain (often >1 m) and rapid vegetation colonisation following restoration, conditions that promoted sustained organic matter accumulation.

Labile and recalcitrant OC exhibited contrasting depth profiles and elevation patterns (Figure 5). Labile OC was concentrated near the surface, peaking in the top 30 cm of High-elevation cores (median = 2.10%, range = 1.11–3.53%), compared to a site-wide median of 1.77% (range = 0.48–3.53%), and declined steeply with depth across all elevation zones (edf = 9.8–16.4, $p < 0.001$), approaching zero below ~40 cm. In contrast, recalcitrant OC was more persistent with depth, showing weaker non-linear trends (edf = 6.7–12.3, $p < 0.001$) and dominating below ~40 cm, consistent with its greater chemical stability. Surface concentrations of recalcitrant OC were highest in the reference marsh (top 30 cm: median = 2.47%, range = 2.11–3.45%), well above the site-wide median of 1.32% (range = 0.27–3.45%), with lower values in the MR. The higher recalcitrant OC in the reference marsh may reflect greater

organic matter inputs associated with its more established vegetation, which could provide more material for stabilisation and humification over time. Elevation contrasts from the fitted models were negative relative to High for both fractions (e.g., Low vs High: labile $\beta = -0.17 \pm 0.03$, $p < 0.001$; recalcitrant $\beta = -0.31 \pm 0.15$, $p = 0.044$; Mid vs High: labile $\beta = -0.04 \pm 0.02$, $p = 0.042$; recalcitrant $\beta = -0.30 \pm 0.14$, $p < 0.05$), reflecting lower surface concentrations in Low/Mid elevation zones. Overall, these patterns suggest that labile OC is strongly influenced by elevation-driven processes and vegetation inputs, while recalcitrant OC represents older, more stable carbon at depth (see Supplementary Table 2 to 4 for full GAM outputs).

*Organic carbon stock and accumulation rates*

Average annual carbon accumulation across cores was 15 $t\,C\,ha^{-1}\,yr^{-1}$ (95% CI: 14.15–16.43), with 4.7 $t\,C\,ha^{-1}\,yr^{-1}$ in the labile fraction (95% CI: 4.34–5.08) and 9.3 $t\,C\,ha^{-1}\,yr^{-1}$ in the recalcitrant fraction (95% CI: 8.18–10.4).

Scaled to the total site area (≈79.8 ha), this equates to a total annual SOC accumulation of 1,206 $t\,C\,yr^{-1}$ (95% CI: 1,117–1,296), including 373 $t\,C\,yr^{-1}$ labile and 732 $t\,C\,yr^{-1}$ recalcitrant carbon. These results account for observed variability among cores in bulk density, OC content, and depth, providing a robust site-wide figure of carbon sequestration at the site.

*Evidence Based Surface Depth for OC Analysis*

Independent empirical criteria converged on a dynamic surface layer near 40 cm, corresponding to the depth interval of greatest variability in sediment properties and the stabilisation of labile OC, and encompassing ≥90% of cumulative OC (Figure 6a). To validate this empirical estimate, segmented regression was applied to the aggregated labile OC profile (Figure 6b). Segmented regression on the aggregated labile-OC profile identified a breakpoint at 40.5 cm (95% CI: 38.4–42.7 cm) (Figure 6b), marking a clear transition from rapid OC decline in the upper layers to a more gradual decrease in deeper sediments (Figure 6b). This closely aligns with the empirical estimate and supports ~40 cm as a representative surface layer for site-wide comparison.

# Discussion

This study provides the first high-resolution, full-depth assessment of OC content in a UK MR site. By resolving vertical profiles, distinguishing labile and recalcitrant fractions, and stratifying by elevation, we avoid biases

from prescribed shallow depths or full-core averaging and quantify how near-surface processes differ from deeper, longer-term storage. We estimate site-wide accumulation of ~15 t C $ha^{-1}$ $yr^{-1}$ (1,206 t C $yr^{-1}$), with deeper strata dominated by recalcitrant OC, consistent with long-term stability.

A consistent pattern across studies suggests that rapidly accumulating MR saltmarsh with low sediment carbon content can achieve similar carbon accumulation rates to slowly accreting marshes with higher carbon densities [47, 48]. In MR sites with limited sediment availability, significantly lower carbon accumulation rates have been recorded. For example, in the Blackwater Estuary (Essex), where suspended sediment concentrations range from 50 to 150 mg $L^{-1}$ (Ladd, 2019), accumulation rates were reported at 3.21 t C $ha^{-1}$ $yr^{-1}$ in Orplands and 3.33 t C $ha^{-1}$ $yr^{-1}$ in Northey Island [23]. Even lower rates were observed in Tollesbury (1.04 t C $ha^{-1}$ $yr^{-1}$), also within the Blackwater Estuary, where reduced sediment delivery compared to other sites and site-specific conditions constrained deposition [3]. In contrast, the Humber Estuary is characterised by large tidal ranges (macrotidal), allowing sediment deposition on both the flood and ebb tides, with one of the highest suspended sediment concentrations in the water column, in the UK (19 - 27 g/L) [49, 50]. Incoming sediment is typically composed of fine silts and clays with moderate to high organic content, depending on tidal conditions [29]. Sites with high sediment supply show markedly higher accumulation rates, for instance, Steart Marsh (Somerset), with suspended sediment concentrations ranging from 1,000 to 10,000 mg/L, recorded an accumulation rate of 19.4 t C $ha^{-1}$ $yr^{-1}$ [12]. Similarly, the upper Bay of Fundy (Canada), where sediment concentrations range from 150 to 300 mg/L [51], reported rates of 13.29 t C $ha^{-1}$ $yr^{-1}$[52].

Per-hectare values of sediment organic carbon are strongly determined by the depth of the organic horizon [53], which is ultimately determined by the rate and carbon density of sediment supply, as well as root material accumulation, which contributes to elevation gain. Elevation change data (Figure 1) highlights substantial variability in sedimentation across Paull Holme Strays, from ~11 cm in high-elevation areas to ~250 cm in low-lying areas near the western breach (Figure 1). Across Paull Holme Strays High-elevation zones with limited sedimentation exhibited higher OC densities but lower overall accumulation rates (Figure 1 and 4), whereas rapidly accreting zones stored less OC per unit mass yet achieved comparable annual accumulation (~15 t C $ha^{-1}$ $yr^{-1}$). This supports the dual role of sediment supply and carbon concentration (i.e. inputs from vegetation), in determining sequestration potential. For example, cores near the western breach contained some of the highest OC stocks (up to 4.1 g $cm^{-2}$), whereas eastern areas rarely exceeded 3 g $cm^{-2}$. These patterns are strongly influenced by hydrodynamic controls, where greater tidal energy and proximity to the breach promote rapid accretion in

western areas, while eastern areas remain more sheltered and accumulate less sediment. Understanding these spatial differences is critical for predicting long-term carbon storage and designing restoration strategies that optimise both sediment delivery and vegetation development. Consequently, equal depths sampled across elevations may reflect different depositional conditions, so fixed-depth comparisons should be interpreted with caution.

The accommodation space created during restoration is often rapidly infilled with sediments originating from adjacent environments, rather than with autochthonous organic matter produced by in-situ saltmarsh vegetation [54]. While the long-term fate of this initial influx has previously been uncertain. However, our depth-resolved analysis revealed a sharp decline in labile OC below ~40 cm (Figure 6), confirmed by segmented regression (breakpoint at 40.5 cm, 95% CI: 38.4–42.7). This transition marks the dynamic surface layer where most OC turnover occurs and coincides with the depth interval of greatest variability in sediment properties. Below this depth, labile OC approaches zero, while recalcitrant OC persists, indicating that long-term carbon storage is dominated by chemically stable fractions. This pattern, supported by a non-linear decline in OC concentrations with depth ($edf = 3.06$, $p < 0.001$), is consistent with post-depositional remineralisation, whereby labile carbon in surface layers is progressively degraded during burial.

It is well-established that vegetation plays a key role in determining SOC levels [55, 56], through direct input of OC from plant roots and decaying biomass, as well as indirectly through vegetation structures, (e.g. leaves, stems), facilitating the trapping of sediment and thus the accumulation of allochthonous OC [57]. Areas of high elevation and dense vegetation are likely to lose more labile carbon over time due to two key factors: first, they tend to receive substantial inputs of labile organic matter from vegetation (both during initial colonisation and subsequent biomass production); and second, they are less frequently inundated, resulting in more oxygenated conditions that accelerate microbial degradation [58]. The significant elevation–depth interaction ($edf = 11.8$, $p < 0.001$) indicates that OC loss with depth was most pronounced in high-elevation zones, consistent with known patterns of microbial degradation where more chemically or biologically labile organic matter is remineralised rather than preserved in long-term carbon stocks [59]. In contrast, low-elevation areas, although storing less OC initially (Figure 5), exhibited slower rates of OC decline. These areas tend to be more frequently inundated and more anoxic which slows down microbial decomposition, favouring the preservation of labile carbon.

By pairing near-unprecedented sampling resolution with elevation-stratified cores and depth-resolved OC fractionation, this study disentangles short-term turnover from longer-term carbon preservation in

restored intertidal habitats. The combination of vertical profiles and fraction-specific dynamics clarifies why low-elevation, rapidly accreting sediments with lower OC concentrations, and high-elevation, OC-dense sediments with little accretion can produce similar annual OC accumulation, a pattern widely observed but previously unexplained in managed-realignment systems. Our empirical identification of a ~40 cm dynamic surface layer provides a practical depth for consistent comparison across heterogeneous elevations, reducing the bias introduced by fixed sampling depths or surface extrapolations. Together, these elements offer a scalable, evidence-based approach to interpreting OC stocks and accumulation across restored intertidal environments, directly addressing longstanding uncertainty around vertical OC persistence and improving the reproducibility and transparency of blue-carbon assessments. By resolving the mechanisms that structure OC variability within a realignment site, this study advances the basis for robust monitoring and strengthens the scientific foundation of coastal-restoration carbon accounting.

*References*


1. Mason, V.G., et al., *Blue carbon benefits from global saltmarsh restoration.* Global Change Biology, 2023. **29**: p. 6517-6545.
2. Barbier, E.B., et al., *The value of estuarine and coastal ecosystem services.* Ecological Monographs, 2011. **81**(2): p. 169-193.
3. Burden, A., A. Garbutt, and C.D. Evans, *Effect of restoration on saltmarsh carbon accumulation in Eastern England.* Biol Lett, 2019. **15**(1): p. 20180773.
4. Lovelock, C.E., et al., *An Australian blue carbon method to estimate climate change mitigation benefits of coastal wetland restoration.* Restoration Ecology, 2022. **31**: p. e13739.
5. Saintilan, N., et al., *Constraints on the adjustment of tidal marshes to accelerating sea level rise.* Science, 2022. **29**(6605): p. 523-527.
6. Pétillon, J., et al., *Top ten priorities for global saltmarsh restoration, conservation and ecosystem service research.* Science of the Total Environment, 2023. **898**: p. 165544.
7. Campbell, A.D., et al., *A review of carbon monitoring in wet carbon systems using remote sensing.* Environmental Research Letters, 2022. **17**(2).
8. Liu, N. and X. Ma, *Ecological restoration of coastal wetlands in China: Current status and suggestions.* Biological Conservation, 2024. **291**(110513).
9. Hudson, R., J. Kenworthy, and M. Best, *Saltmarsh Restoration Handbook: UK and Ireland.* 2021.
10. French, P.W., *Managed realignment – The developing story of a comparatively new approach to soft engineering.* Estuarine, Coastal and Shelf Science, 2006. **67**(3): p. 409-423.
11. Wollenberg, J.T., J. Ollerhead, and G.L. Chmura, *Rapid carbon accumulation following managed realignment on the Bay of Fundy.* PLoS One, 2018. **13**(3): p. e0193930.

12. Mossman, H.L., et al., *Rapid carbon accumulation at a saltmarsh restored by managed realignment exceeded carbon emitted in direct site construction.* PLoS One, 2022. **17**(11): p. e0259033.
13. Jimenez-Arias, J.L., et al., *Tidal elevation is the key factor modulating burial rates and composition of organic matter in a coastal wetland with multiple habitats.* Sci Total Environ, 2020. **724**: p. 138205.
14. Mossman, H.L., et al., *Does managed coastal realignment create saltmarshes with 'equivalent biological characteristics' to natural reference sites?* Journal of Applied Ecology, 2012. **49**(6): p. 1446-1456.
15. Spencer, K.L., et al., *The impact of pre-restoration land-use and disturbance on sediment structure, hydrology and the sediment geochemical environment in restored saltmarshes.* Science of the Total Environment, 2017. **587**: p. 47-58.
16. Mazarrasa, I., et al., *Drivers of variability on Blue Carbon stocks and burial rates across European estuarine habitats.* Science of the Total Environment, 2023. **886**.
17. Gore, C., et al., *Saltmarsh blue carbon accumulation rates and their relationship with sea-level rise on a multi-decadal timescale in northern England.* Estuarine Coastal and Shelf Science, 2024. **299**: p. 108665.
18. McLeod, E., et al., *A blueprint for blue carbon: toward an improved understanding of the role of vegetated coastal habitats in sequestering CO2.* Frontiers in Ecology and the Environment, 2011. **9**(10): p. 552-560.
19. Van de Broek, M., Temmerman, S., Merckx, R., Gover, G, *Controls of soil organic carbon stocks in tidal marshes along an estuarine salinity gradient.* Biogeosciences, 2016. **13**: p. 6611-6624.
20. Ford, H., et al., *Large-scale predictions of salt-marsh carbon stock based on simple observations of plant community and soil type.* Biogeosciences, 2019. **16**(2): p. 425-436.
21. van Ardenne, L.B., et al., *High resolution carbon stock and soil data for three salt marshes along the northeastern coast of North America.* Data Brief, 2018. **19**: p. 2438-2441.
22. Miller, C.B., et al., *Carbon accumulation rates are highest at young and expanding salt marsh edges.* Communications Earth & Environment, 2022. **3**(1).
23. McMahon, L., et al., *Maximizing blue carbon stocks through saltmarsh restoration.* Frontiers in Marine Science, 2023. **10**: p. 1106607.
24. Ouyang, X. and S.Y. Lee, *Updated estimates of carbon accumulation rates in coastal marsh sediments.* Biogeosciences, 2014. **11**(18): p. 5057-5071.
25. Chmura, G.L., et al., *Global carbon sequestration in tidal, saline wetland soils.* Global Biogeochemical Cycles, 2003. **17**(4): p. n/a-n/a.
26. Beaumont, N.J., et al., *The value of carbon sequestration and storage in coastal habitats.* Estuarine Coastal and Shelf Science, 2014. **137**: p. 32-40.
27. Smeaton, C., et al., *Using citizen science to estimate surficial soil Blue Carbon stocks in Great British saltmarshes.* Frontiers in Marine Science, 2022. **9**.
28. Leorri, E., et al., *Refractory organic matter in coastal salt marshes-effect on C sequestration calculations.* Science of the Total Environment, 2018. **633**: p. 391-398.
29. Mazik, K., et al., *Physical and biological development of a newly breached managed realignment site, Humber estuary, UK.* Mar Pollut Bull, 2007. **55**(10-12): p. 564-78.
30. Lonsdale, J.-A., et al., *Managing estuaries under a changing climate: A case study of the Humber Estuary, UK.* Environmental Science and Policy., 2022. **134**: p. 75-85.

31. Defra. *LiDAR Composite DTM-0.5m.* 2022.
32. Howard, J., et al., *Coastal Blue Carbon: Methods for assessing carbon stocks and emissions facotrs in mangroves, tidal salt marshes, and seagrasses.* 2012, Conservation International, Intergovernmental Oceanographic Comission of UNESCO, International Union for Conservation of Nature.: Arlington, Virginia, USA.
33. Al-Shammary, A.A.G., et al., *Soil Bulk Density Estimation Methods: A Review.* Pedosphere, 2018. **28**(4): p. 581-596.
34. Howard, J., et al., *Coastal Blue Carbon: Methods for assessing carbon stocks and emissions factors in mangroves, tidal salt marshes, and seagrass meadows*. 2014, Conservation International, Intergovernmental Oceanographic Commission of UNESCO, International Union for Conservation of Nature.: Arlington, Virginia, USA.
35. Breithaupt, J.L., et al., *An Improved Framework for Estimating Organic Carbon Content of Mangrove Soils Using loss-on-ignition and Coastal Environmental Setting.* Wetlands, 2023. **43**: p. 57.
36. Polakowski, C., et al., *Recommendations for soil sample preparation, pretreatment, and data conversion for texture classification in laser diffraction particle size analysis.* Geoderma, 2023. **430**: p. 116358.
37. Folk, W. and W.C. Ward, *Brazos River bar: a study in the significance of grain size parameters.* Journal of Sedimentary Research, 1957. **27**: p. 3-26.
38. Blott, S.J. and K. Pye, *GRADISTAT: a grain size distribution and statistics package for the analysis of unconsolidated sediments.* Earth Surface Processes and Landforms, 2001. **26**(11).
39. Pryor, E.J., et al., *Recommended centrifuge method: Specific grain size separation in the <63 µm fraction of marine sediments.* MethodsX, 2024. **12**(102718).
40. Nayak, A.K., et al., *Current and emerging methodologies for estimating carbon sequestration in agricultural soils: A review.* Science of the Total Environment, 2019. **665**: p. 890-912.
41. Serrano, O., et al., *Flaws in the methodologies for organic carbon analysis in seagrass blue carbon soils.* Limnology & Oceanography: Methods, 2023. **21**: p. 814-827.
42. Fu, H., et al., *A comparative study of methods for determining carbonate content in marine and terrestrial sediments.* Marine and Petroleum Geology, 2020. **116**: p. 104337.
43. RCoreTeam, *R: A language and environment for statistical computing.* , in *R Foundation for Statistical Computing*. 2023: Vienna, Austria.
44. Wickham, H., *ggplot2: Elegant graphics for data analysis*. 2016, New York: Springer-Verlag.
45. Wood, S.N., *mgcv: Mixed GAM Computation Vehicle with Automatic Smoothness Estimation.* . 2023.
46. Canty, A. and B.D. Ripley, *boot: Bootstrap Functions (Originally by Angelo Canty for S)*, in *R package version 1.3-28*. 2023.
47. Amann, B., et al., *Multi-annual and multi-decadal evolution of sediment accretion in a saltmarsh of the French Atlantic coast: Implications for carbon sequestration.* Estuarine Coastal and Shelf Science, 2023. **293**: p. 108467.
48. Benjamin, A., et al., *Understanding sediment and carbon accumulation in macrotidal minerogenic saltmarshes for climate resilience.* Geomorphology, 2024. **467**: p. 109465.
49. Uncles, R.J., J.A. Stephens, and R.E. Smith, *The dependence of estuarine turbidity on tidal intrusion length, tidal range and residence time.* Continental Shelf Research, 2002. **22**(11-13): p. 1835-1856.

50. Morris, R.K.A. and S.B. Mitchel, *Has Loss of Accommodation Space in the Humber Estuary Led to Elevated Suspended Sediment Concentrations? .* Journal of Frontiers in Construction Engineering, 2013. **2**(1): p. 1-9.
51. Schostak, L.E., et al., *Patterns of flow and suspended sediment concentration in a macrotidal saltmarsh creek, Bay of Fundy, Canada*, in *Coastal and Estuarine Environments: Sedimentology, Geomorphology and Geoarchaeology*, K. Pye and J.R.L. Allen, Editors. 2000, Geological Society of London. p. 0.
52. Wollenburg, J.T., J. Ollerhead, and G.L. Chmura, *Rapid carbon accumulation following managed realignment on the Bay of Fundy.* PLoS One, 2018. **13**: p. e0193930.
53. Pye, K. and S.J. Blott, *The geomorphology of UK estuaries: The role of geological controls, antecedent conditions and human activities.* Estuarine Coastal and Shelf Science, 2014. **150**: p. 196-214.
54. Saintilan, N.S., et al., *Allochthonous and autochthonous contributions to carbon accumulation and carbon store in southeastern Australian coastal wetlands.* Estuaries and Coastal Shelf Science, 2013. **128**: p. 84-92.
55. Duarte, C.M., et al., *The role of coastal plant communities for climate change mitigation and adaptation.* Nature Climate Change, 2013. **3**(11): p. 961-968.
56. Kelleway, J.J., et al., *Sediment and carbon deposition vary among vegetation assemblages in a coastal salt marsh.* Biogeosciences, 2017. **14**(16): p. 3763-3779.
57. Mudd, S.M., A. D'Alpaos, and J.T. Morris, *How does vegetation affect sedimentation on tidal marshes? Investigating particle capture and hydrodynamic controls on biologically mediated sedimentation.* Journal of Geophysical Research, 2010. **115**: p. F03029.
58. Hill, A.C. and R. Vargas, *Methane and Carbon Dioxide Fluxes in a Temperate Tidal Salt Marsh: Comparisons Between Plot and Ecosystem Measurements.* JGR Biogeosciences, 2022. **127**(7): p. e2022JG006943.
59. Belshe, E.F., et al., *Modeling organic carbon accumulation rates and residence times in coastal vegetated ecosystems.* Journal of Geophysical research: Biogeosciences, 2019. **124**(11): p. 3652-3671.

# Figures

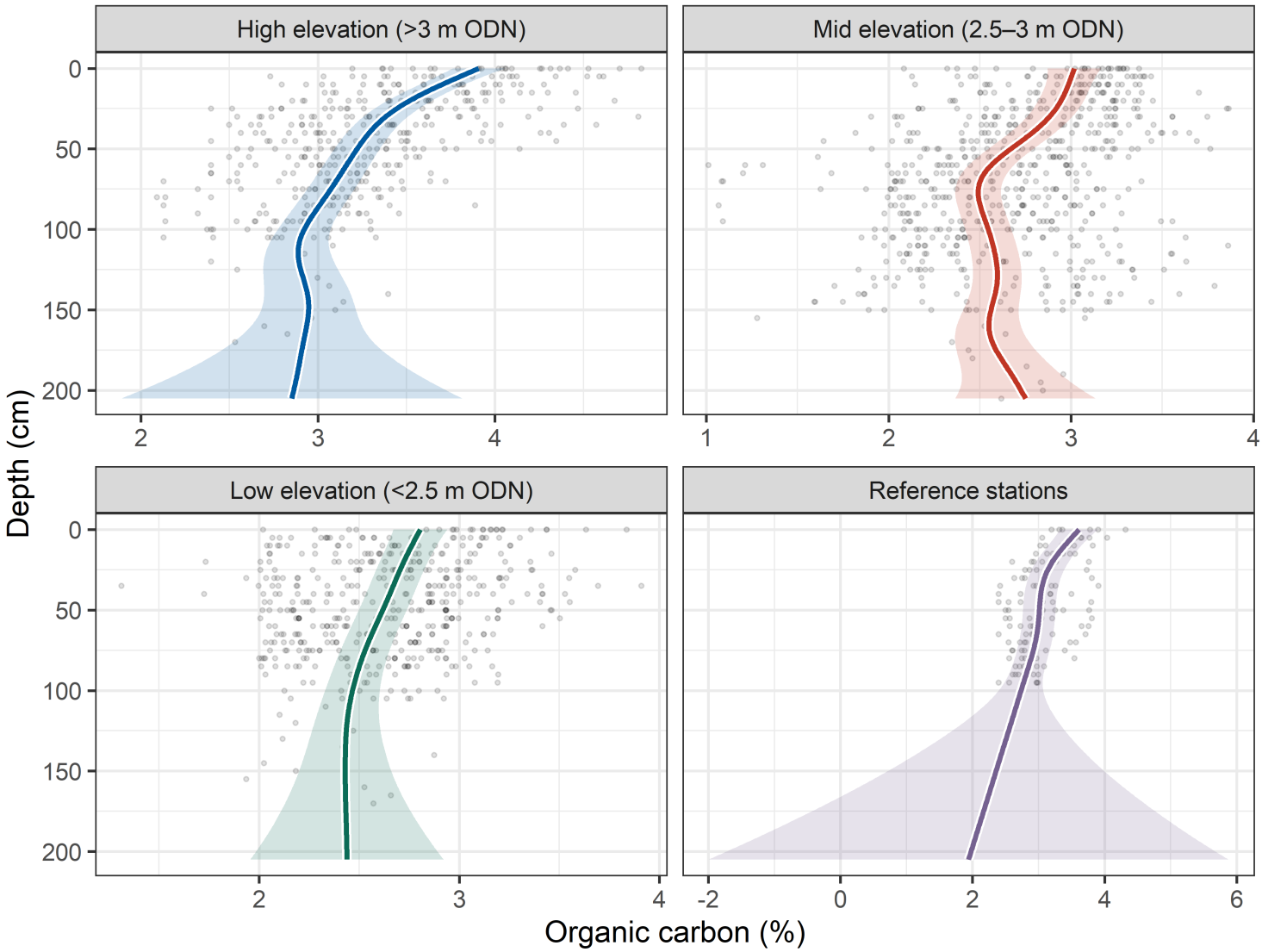



**Figure 1**

Figure 3

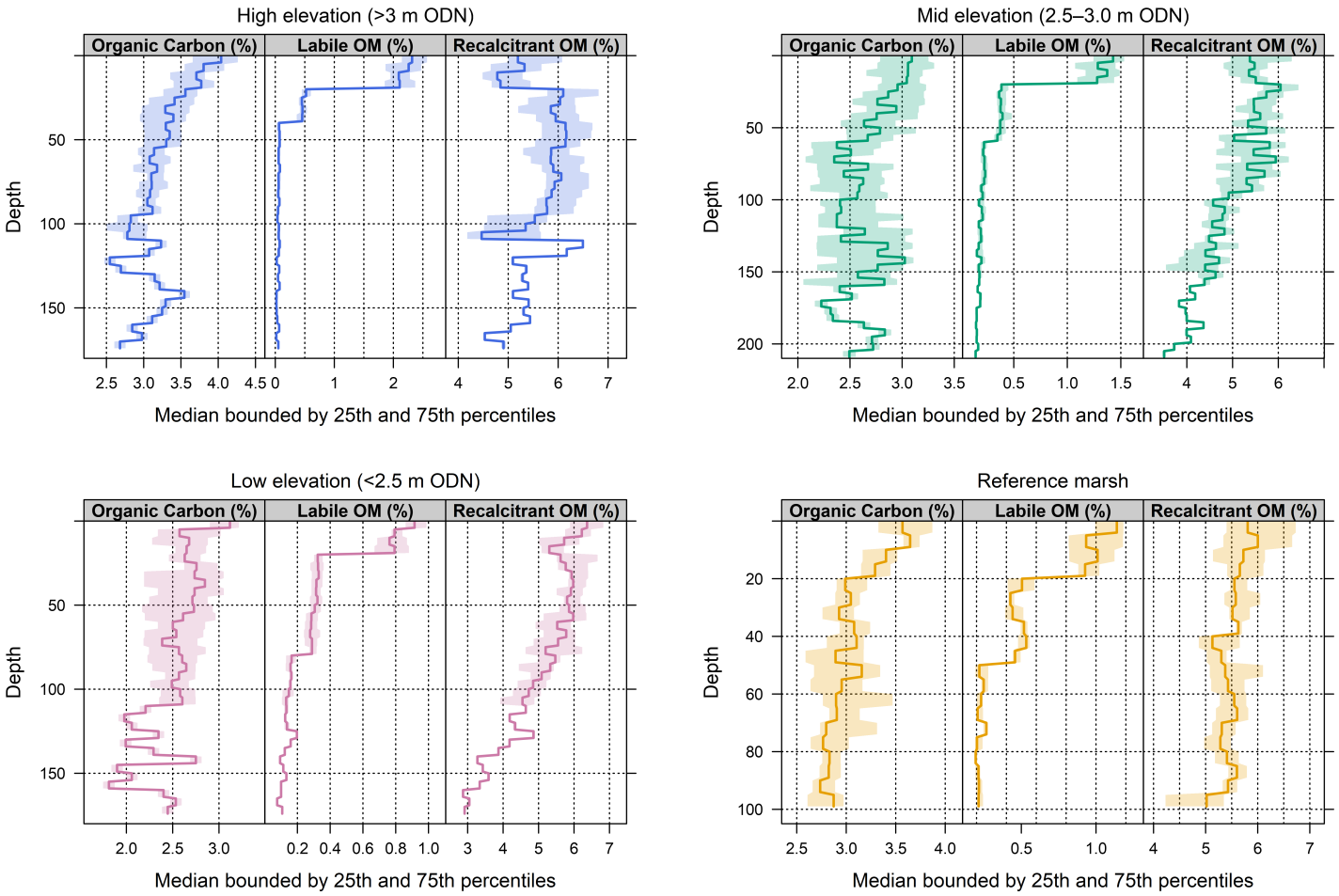



**Figure 2**

Figure 5

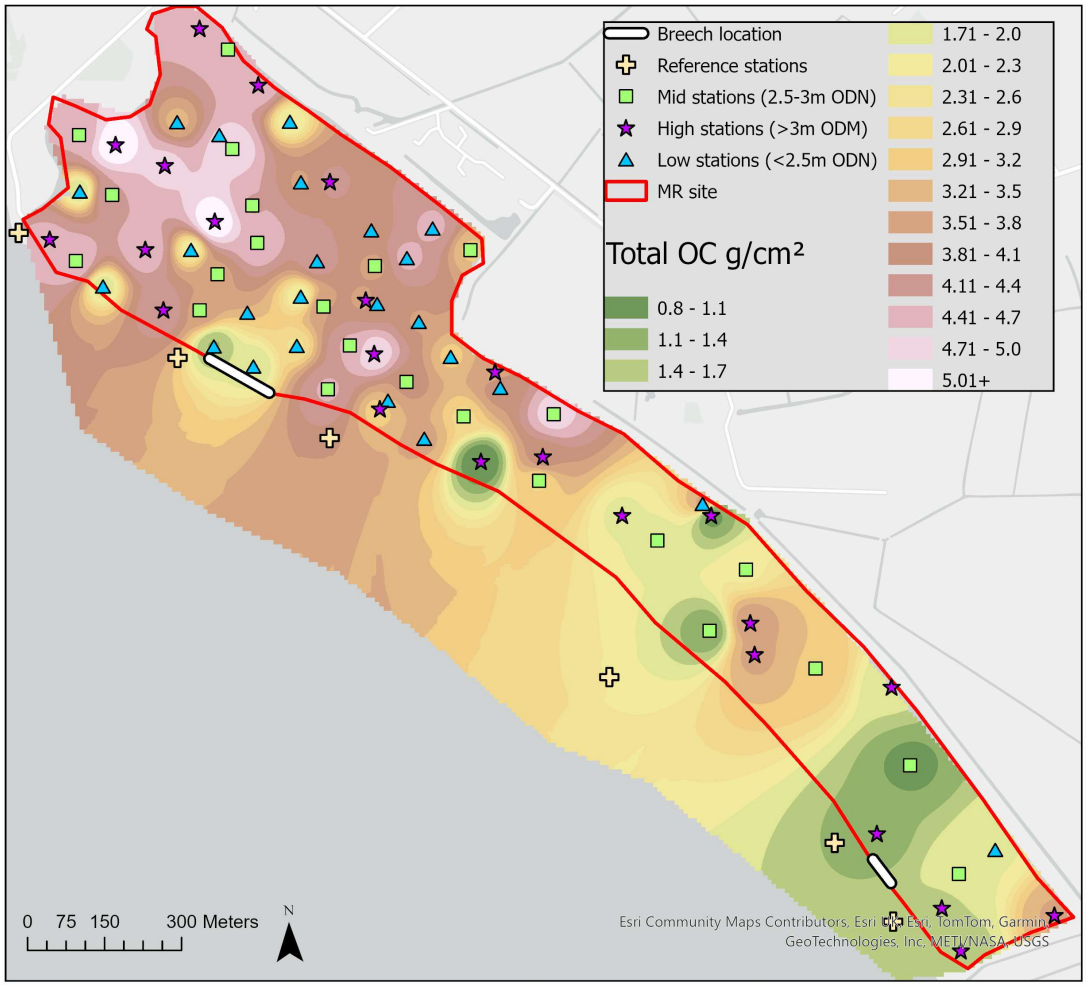



**Figure 3**

Figure 4



**Figure 4**

2a-d

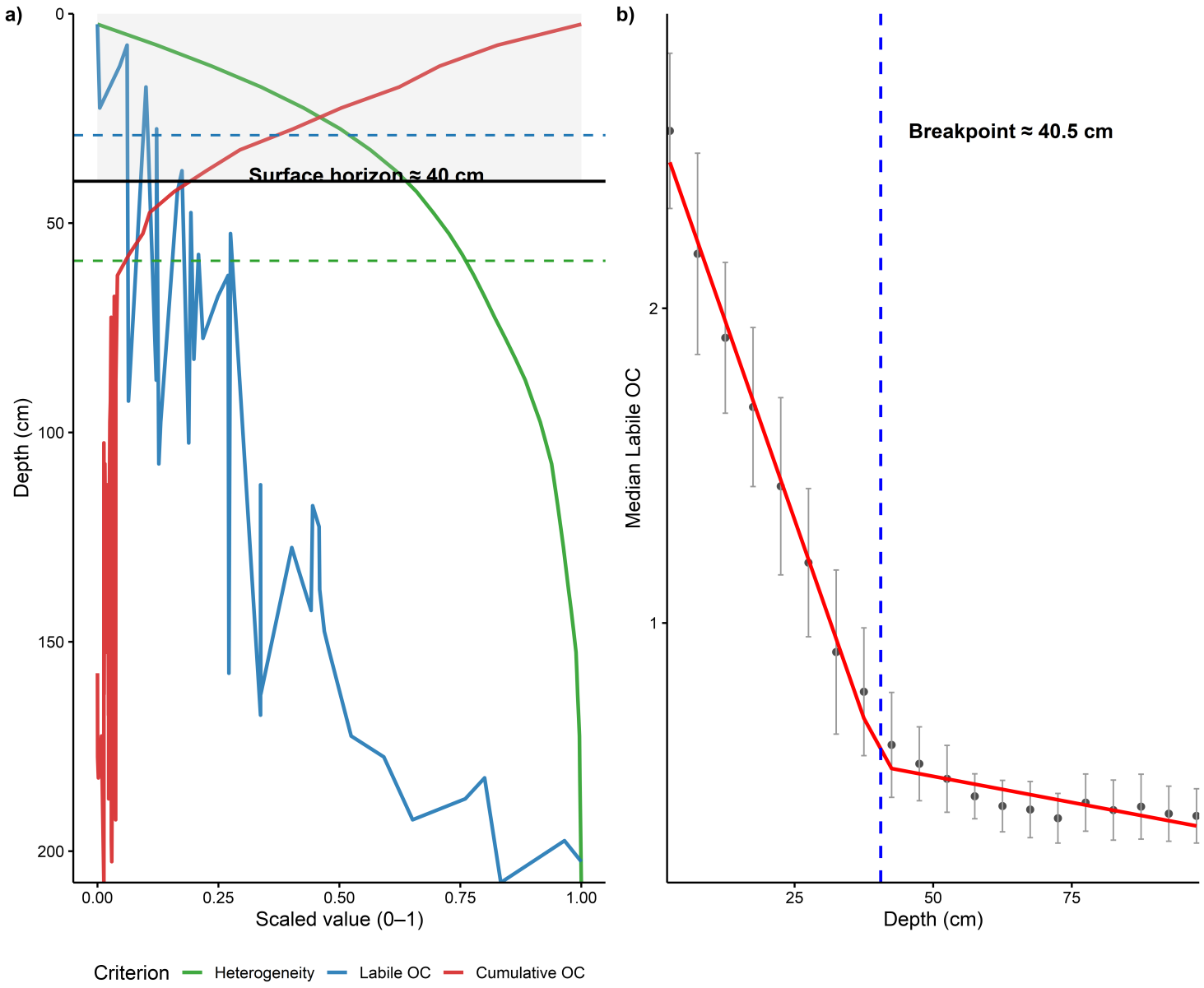



**Figure 5**

6 a and b

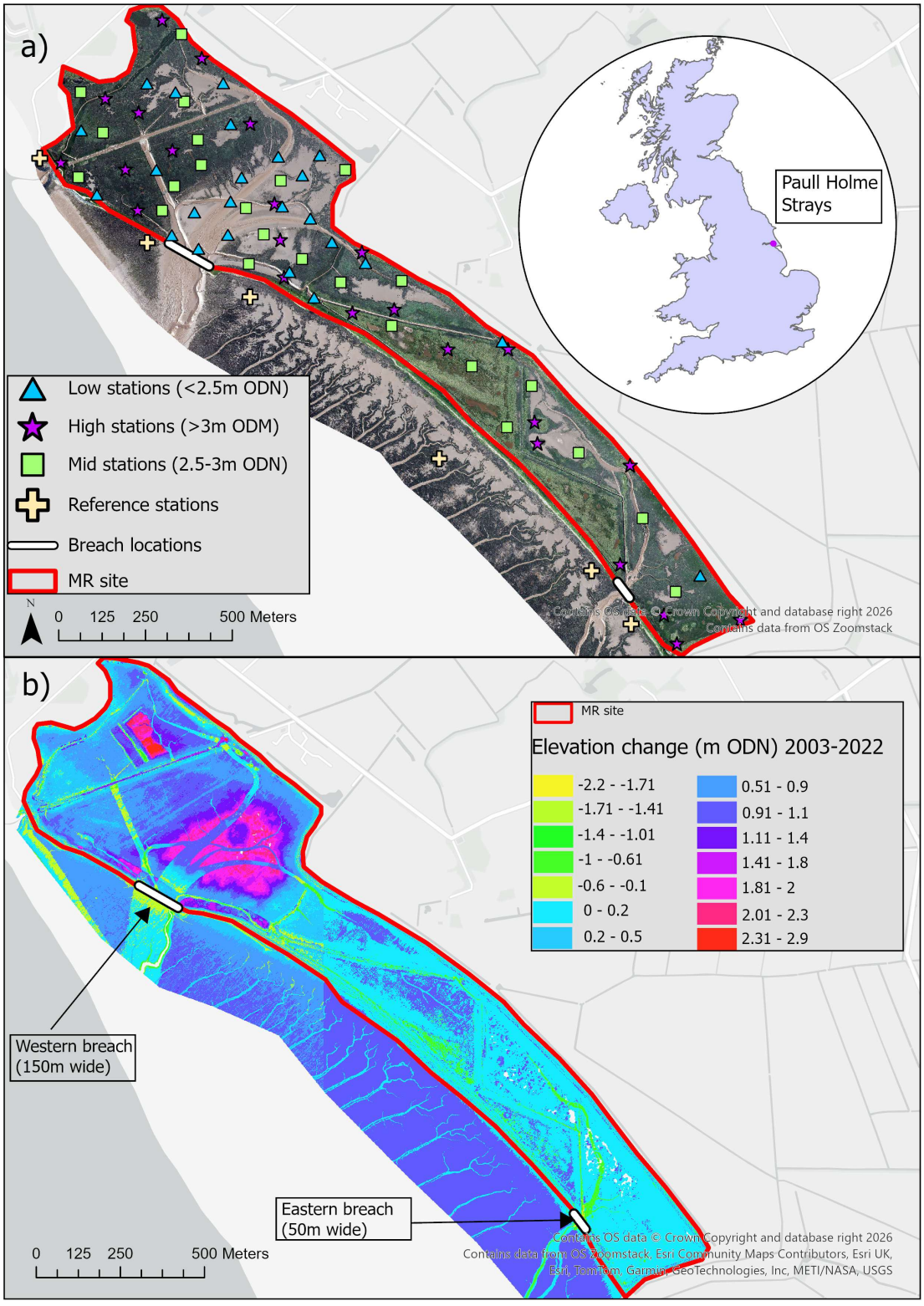



**Figure 6**

1a and b

# Supplementary Files

This is a list of supplementary files associated with this preprint. Click to download.

- SupplementaryInformation.docx
- Rscript.docx